Supplementary Material

Novel COF-based core-shell material UiO@BTT-BPDA as an adsorbent for efficient and rapid removal of persistent organic pollutants

Rong Ma [a], *Yuanyuan Li* [a*], *Xiaomei Yu* [a], *Rumei Jia* [a], *Yulong Ma* [a], *Yonggang Sun* [a], *Wenxin Ji* [a]

[a] *State Key Laboratory of High-efficiency Utilization of Coal and Green Chemical Engineering, College of Chemistry and Chemical Engineering, Ningxia University, Yinchuan 750021, China*

[*]*Corresponding Author: E-mail: liyuanyuan_abc-sohu.com (Yuanyuan Li)*

Tel: +86-951-2062330; Fax: +86-951-2062323

Materials

In our experiments, the required ingredients include benzotrithiophene tricarbaldehyde (BTT), [2,2'-bipyridine]-5,5'-diamine (BPDA), zirconium tetrachloride ($ZrCl_4$), tetrahydrofuran (THF), methanol (MeOH), acetic acid (HAc), 1,4-dioxane, N,N-dimethylformamide (DMF), 2-aminoterephthalic acid and 2,5-dihydroxyterephthalic acid were supplied by Aladdin Chemistry Co. Ltd. (Shanghai, China).CR ($C_{32}H_{22}N_6Na_2O_6S_2$, 99.0%), MG ($C_{23}H_{25}ClN_2$, 99.0%) and RB ($C_{28}H_{31}ClN_2O_3$, 99.0%), all purchased from Sinopharm Chemical Reagent Co. Ltd. China. All the chemicals are of analytical grade without any further treatment. Deionized water (DI) was used throughout the experiments.

Characterization

X-ray powder diffraction (XRD) analysis (Bruker, Cu-Kα, λ = 1.5418 Å) was used to describe the crystallinity and crystal structure of the samples. FTIR spectra was recorded in the range of 400-4000 cm^{-1}(Mattson Satellite Infrared Spectrometer). X-ray photoelectron spectroscopy (XPS) (Shimadzu Axis Supra, Al Kα) was used to characterize the surface elemental composition. The surface morphology was presented by SEM (JEOL, JSM-F100). Auto Specific Surface Area and Porosity Analyzer (Micromeritics, ASAP2460)，Talos F200C at an accelerating voltage of 100 kV was applied to keep track of TEM images.

Adsorption experiments

A typical adsorption test was performed by adding 5 mg adsorbent to a 20 mL vial containing certain concentrations of adsorbates (RB, CR and MG) solutions. The vials were ultrasonicated for 5 minutes, then moved to a shaking table and oscillated at 298 K for 2 h. Next, let the solution stand for about 1 h, the solid–liquid mixture can be separated. Thus, the residual concentration of sorbents was determined

by UV–Vis spectrometer at 554, 497 and 617 nm for RB, CR and MG. Experimental details and equations are shown in supplementary material.

Batch adsorption experiments were used to investigate the effects of initial solution pH, contact time, ambient temperature and initial concentration of adsorbent on the removal of RB, CR and MG. Typically, 5 mg of adsorbent was added to a vial containing 20 mL of adsorbent solution. The vials were transferred to a shaking table and oscillated at 298 K for 2h to complete the adsorption process. The effect of initial solution pH was studied by changing the solution pH (2-12) with 0.1 M hydrochloric acid and 0.1 M sodium hydroxide. To study the adsorption kinetics, the residual concentrations of adsorbed masses were detected at predetermined time points (3,5, 10, 15, 30, 60, 120, 240, 320 and 360 min) during the adsorption process. To investigate the adsorption isotherms, different initial concentrations were tested for each dye: methylene blue (MG) and rhodamine B (RB) at 100–500 mg/L (in 100 mg/L increments), while Congo red (CR) was studied at lower concentrations (50–250 mg/L in 50 mg/L increments). After 240 minutes of adsorption, the residual dye concentrations were measured to determine the adsorption capacity. Experiments were conducted at three different temperatures (298 K, 308 K, 318 K) to investigate the effect of ambient temperature on adsorption. After the adsorption, the solid-liquid mixture was separated by natural standing and the concentration of adsorbed substances was measured with a UV-Vis spectrometer (PERSEE, TU-1901) at 554, 497 and 617 nm, respectively. The concentration was calculated as follows:

$$q_t = \frac{(C_0 - C_t)V}{m}, \qquad (1)$$

$$q_e = \frac{(C_0 - C_e)V}{m}, \qquad (2)$$

where C_0 (mg L^{-1}) is the initial concentration of the dye solutions, C_t and C_e (mg L^{-1}) represent the concentration of the residual adsorbates at a certain time and adsorption equilibrium respectively, q_t or

q_e (mg g^{-1}) are the adsorption capacities at a certain time t or the adsorption equilibrium, m (g) is the mass of the as-used adsorbent, and V (L) is the volume of the solutions.

Adsorption kinetics

To explore the adsorption mechanism, several kinetic models were applied to analyze adsorption processes, including pseudo-first-order, pseudo-second-order and intraparticle diffusion models. The corresponding equations are expressed as follows:

$$log(q_e - q_t) = logq_e - \frac{k_1 t}{2.303}, \quad (3)$$

$$\frac{t}{q_t} = \frac{1}{k_2 q_e^2} + \frac{t}{q_e}, \quad (4)$$

$$q_t = K_i\sqrt{t} + I, \quad (5)$$

where q_e (mg g^{-1}) are the adsorption capacity at equilibrium, k is the rate constants of the kinetic model, h (mg g^{-1} min^{-1}) can be defined as $h = k_2 q_e^2$ at $t \rightarrow 0$, K_i (mg·(g·$min^{1/2}$)$^{-1}$) is the intraparticle diffusion rate constant, and I (mg·g^{-1}) is related to the thickness of the boundary layer.

Adsorption isotherms

To reveal the interaction between the adsorbent and the adsorbates, the adsorption isotherm of the adsorbent was investigated. In this study, the adsorption isotherms were fitted by Langmuir, Freundlich models.

The Langmuir isotherm can be written as

$$q_e = \frac{K_L q_m C_e}{1 + K_L C_e}, \quad (6)$$

$$R_L = \frac{1}{1 + K_L C_0}, \quad (7)$$

where q_m (mg g^{-1}) is the maximum adsorption capacity assuming the monolayer adsorption, K_L (L/mg) is the Langmuir constant and R_L, the equilibrium parameter, is used to reflect the basic properties of the Langmuir isotherm. The equation can be linearized as

$$\frac{C_e}{q_e} = \frac{C_e}{q_m} + \frac{1}{K_L q_m}, \qquad (8)$$

The Freundlich isotherm can be written as

$$q_e = K_F C_e^{1/n}, \qquad (9)$$

where K_F (L mg^{-1}) is the Freundlich constant, and $1/n$ is the adsorption intensity. The equation can be linearized as

$$lnq_e = lnK_F + \frac{1}{n} lnC_e, \qquad (10)$$

Adsorption thermodynamics

The corresponding thermodynamic equations are listed as follows

$$\Delta G = \Delta H - T\Delta S, \qquad (11)$$

$$lnK_c = \frac{\Delta S}{R} - \frac{\Delta H}{RT}, \qquad (12)$$

where ΔG represents the change in the Gibbs free energy, ΔH is the enthalpy change, and ΔS is the entropy change, $K_c = q_e / C_e$, R = 8.314 Jmol^{-1} K^{-1}, and T (K) is the experimental temperature in Kevin.

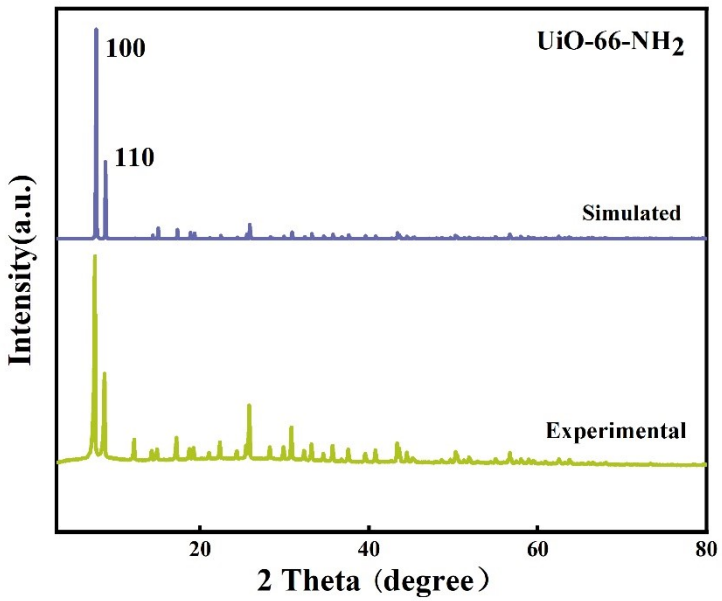

Fig. S1. XRD patterns of UiO-66-NH_2

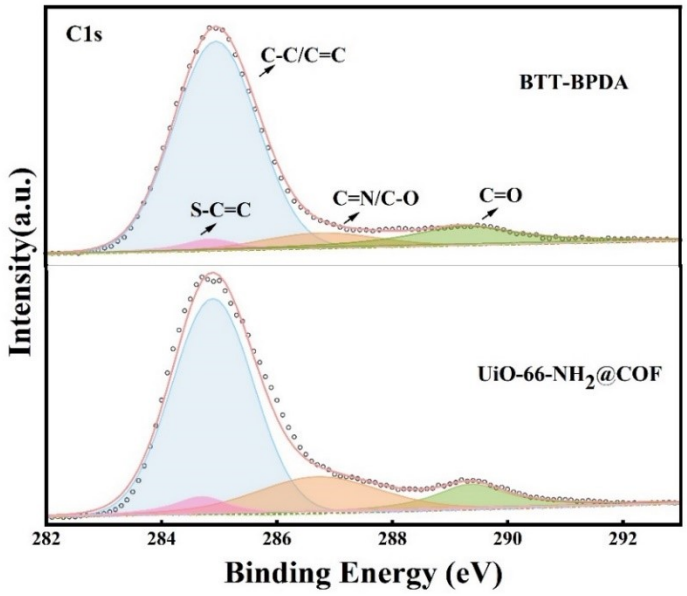

Fig. S2. High-resolution C 1s XPS spectra of BTT-BPDA COF and UiO-66-NH_2@BTT-BPDA.

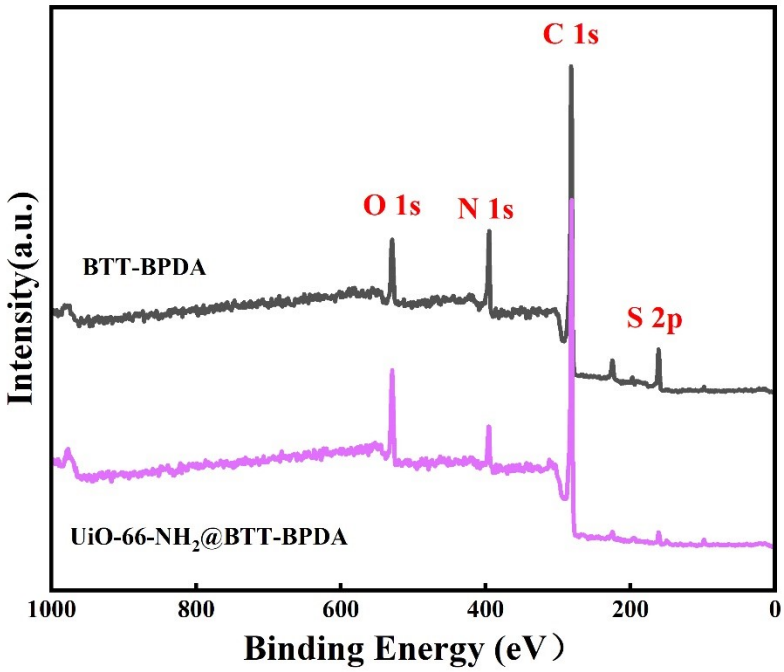

Fig. S3. XPS spectrum of BTT-BPDA and UiO-66-NH_2@BTT-BPDA

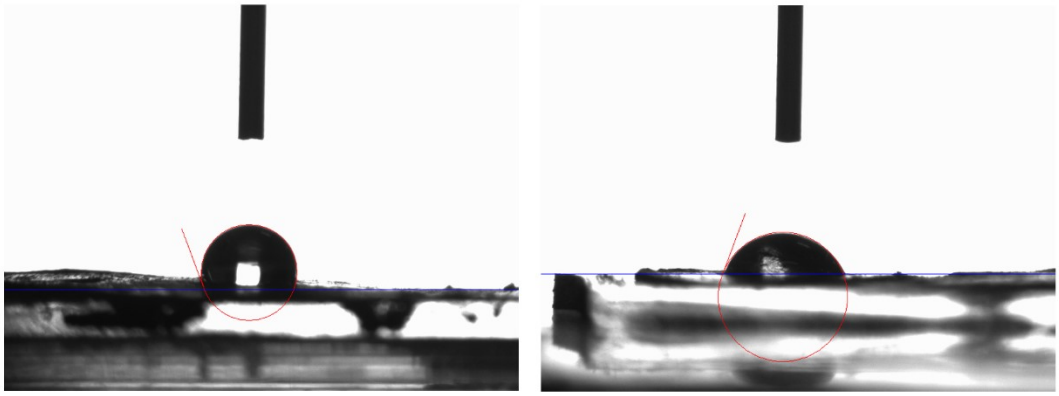

BTT-BPDA -108.425°　　UiO-66-NH_2@BTT-BPDA-73.903°

Fig. S4. Contact angle measurements of BTT-BPDA and UiO-66-NH_2@BTT-BPDA.

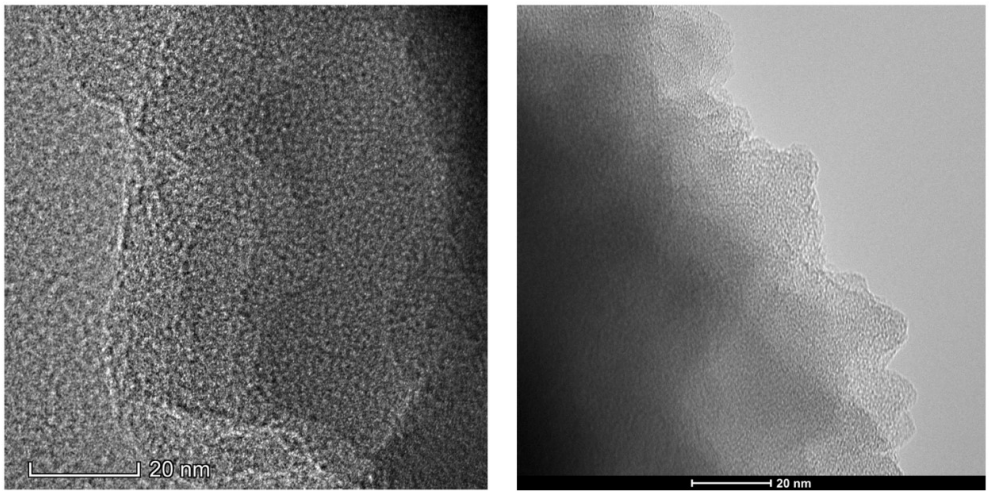

Fig. S5. TEM image of BTT-BPDA

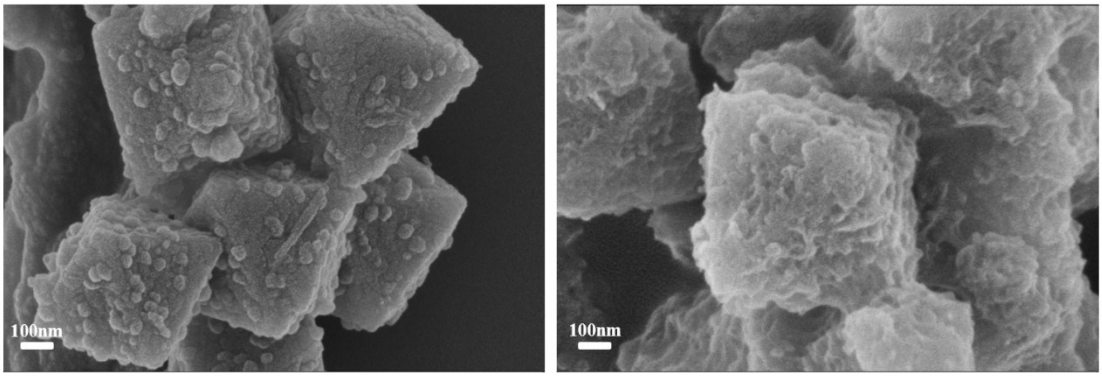

Fig. S6. SEM images of UiO-66-NH_2@BTT-BPDA

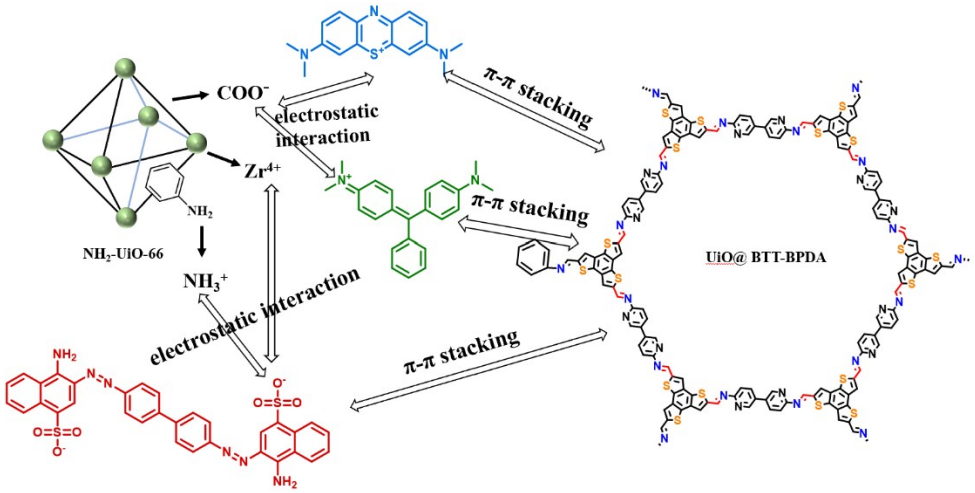

Fig. S7 Possible mechanism of dyes adsorptions on UiO-66-NH_2@BTT-BPDA

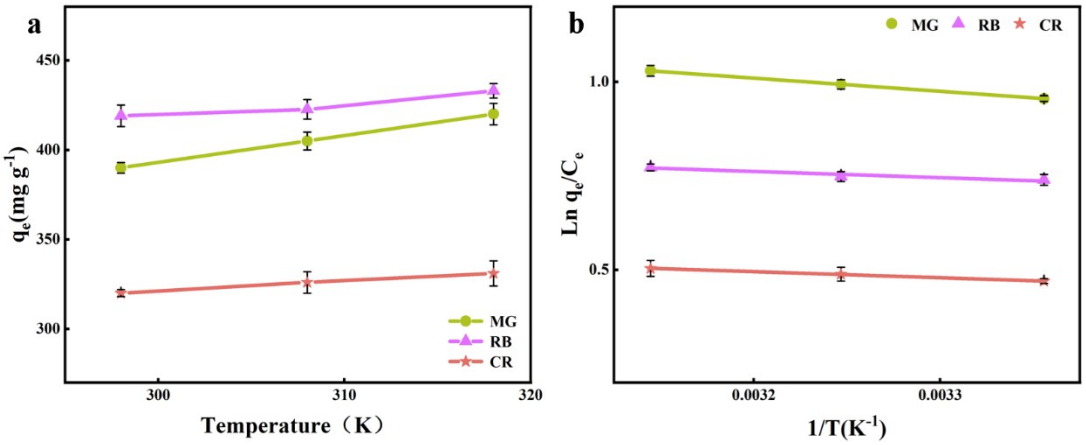

Fig. S8. (a) Effect of temperature and (b) the Van's Hoff equation model for the adsorption process by UiO-66-NH_2@BTT-BPDA.

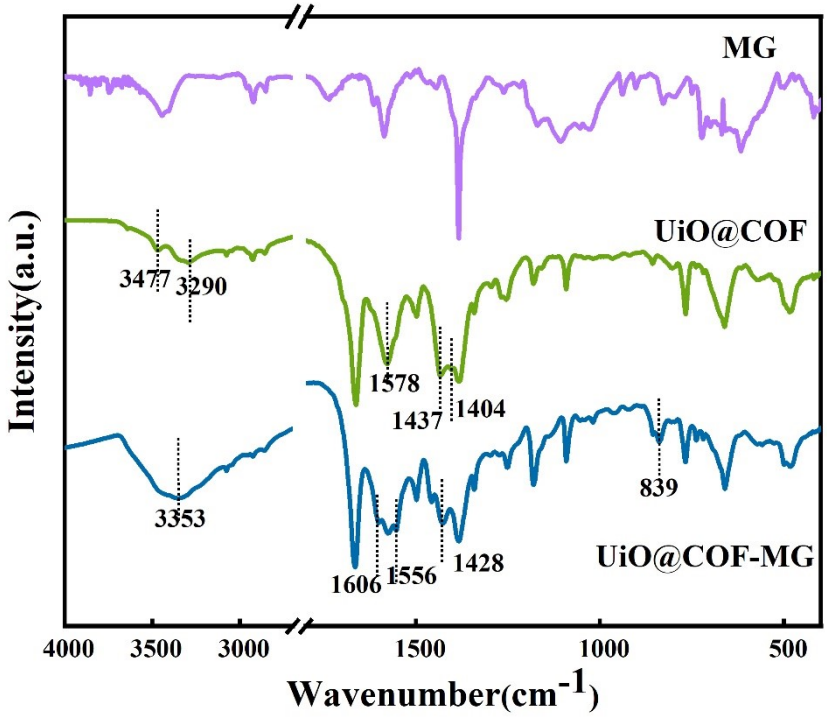

Fig. S9. FT-IR spectra of BTT-BPDA, UiO @COF and UiO @COF after adsorption of MG.

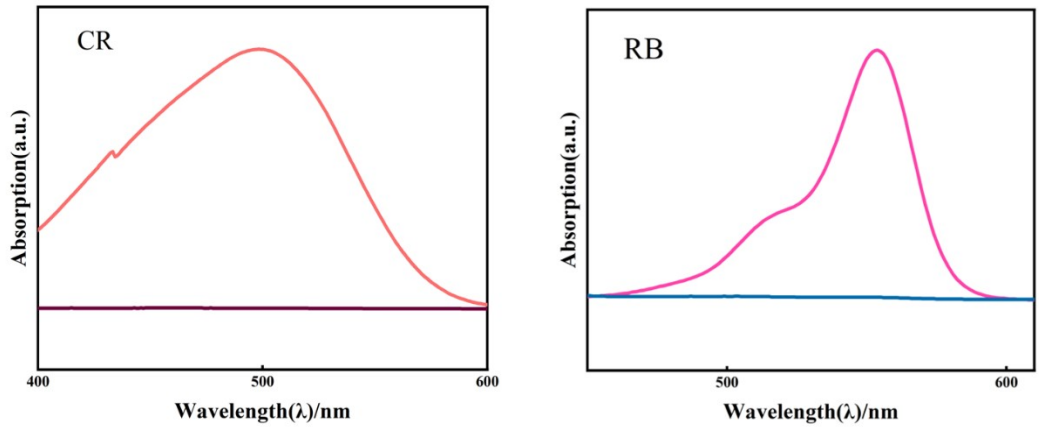

Fig. S10. Comparison of UV visible absorption spectra between the original solution and the adsorbed solution

Table S1 Fractional atomic coordinates for BTT-DPDA COF: space group P 6/m; a=b= 37.013 Å, c=3.535 Å; alpha=beta=90°, gamma=120°

Atom	x (Å)	y (Å)	z (Å)
C1	0.37048	0.66577	0
C2	0.33274	0.62863	0
S3	0.41503	0.75234	0
C4	0.38279	0.7735	0
C5	0.3406	0.74449	0
C6	0.18136	0.57981	0
N7	0.84502	0.40678	0
C8	0.88933	0.43344	0
N9	0.90675	0.47557	0
C10	0.94875	0.5016	0
C11	0.97655	0.4857	0
C12	0.95817	0.44172	0
C13	0.91488	0.41592	0
H14	0.31587	0.75204	0
H15	0.17055	0.54667	0
H16	0.95948	0.53446	0
H17	0.97621	0.42624	0
H18	0.90099	0.38235	0

Table S2. Summary of the nitrogen adsorption/desorption measurement results of all materials.

	BET surface area (m^2/g)	Average pore diameter (nm)
BTT-BPDA	63.2	5.1
UiO-66-NH_2	668.5	2.1
UiO-66-NH_2@BTT-BPDA	181.5	4.1

Table S3. Crystallite size determination for compounds BTT-BPDA and UiO-66-NH_2@BTT-BPDA using the Scherrer equation.

材料	（hkl）晶面	2θ (°)	FWHM (°)	晶粒尺寸 (nm)
UiO-66-NH_2	(100)	7.3	0.68	58.3
UiO-66-NH_2	(110)	8.4	0.18	42.7
BTT-BPDA	(100)	2.8	0.32	26.3
BTT-BPDA	(110)	4.8	0.25	32.6

Table S4. Comparison of UiO-66-NH_2@BTT-BPDA with some other adsorbents recently reported.

Materials	Target	q_{max} (mg g^{-1})	Equilibrium time (h)	Temp. (K)	pH	Refs.
Fe_3O_4@ ZTB-1	CR	458	2	308	7	[1]
ZIF-8@ZIF-67	CR	291.5	1	273	8	[2]
AA-alk-MXene	CR	264.4	1.5	308	7	[3]
MABC-P50	CR	435.9	2.5	298	6.5	[4]
U@BTT-BPDA	CR	1001.3	4	308	7	This work
COF-CTTD	RB	684.9	2	303	7	[5]
PDA-Ttba-COF	RB	833	2	303	7	[6]
silicate/carbon	RB	244	2	328	7	[7]
MIL-68(Al)	RB	1111	1.5	308	7	[8]
U@BTT-BPDA	RB	1616.8	4	308	7	This work
CS-ZIF-2	MG	344.8	3	308	7	[9]
ZIF-8@CS/PVA-ENF	MG	1000	3	308	6	[10]
ZIF-L/NF	MG	5103	2	293	7	[11]
KGM/ZIF-67	MG	2891.3	3.5	303	7	[12]
U@BTT-BPDA	MG	1837.3	4	308	7	This work

Table S5 COD value of Initial and final of MB, RB and CR dye.

Organic dye	Concentration of dye (ppm)	Initial COD (mg/L)	Final COD (mg/L)	Removal efficiency (%)
RB	100	201.44	27.24	86.50
MG	100	221.39	16.13	92.71
CR	100	142.52	25.51	82.10

References

1. L. Han, F. Yuan, G. Sun, X. Gao and H. Zheng, *Dalton transactions (Cambridge, England : 2003)*, 2019, **48**, 4650-4656.
2. C. Gu, W. Weng, C. Lu, P. Tan, Y. Jiang, Q. Zhang, X. Liu and L. Sun, *Chinese Journal of Chemical Engineering*, 2022, **42**, 42-48.
3. Y. Liu, Y. Huo, X. W. B, S. Yu, Y. Ai, Z. Chen, P. Zhang, L. Chen, G. Song and N. S. Alharbi, *Journal of Cleaner Production*, 2020, **278**, 123216.
4. P. Karthikeyan, KrishnapillaiPandi, KalimuthuFayyaz, AqsaMeenakshi, SankaranPark, Chang Min, *CERAMICS INTERNATIONAL*, 2021, **47**, 3692-3698.
5. Q. Jiang, H. Huang, Y. Tang, Y. Zhang and C. Zhong, *Industrial & Engineering Chemistry Research*, 2018, **57**, 15114-15121.
6. T. Xu, S. An, C. Peng, J. Hu and H. Liu, *Industrial & Engineering Chemistry Research*, 2020, **59**, 8315-8322.
7. Z. Sun, X. Duan, C. Srinivasakannan and J. Liang, *RSC Advances*, 2018, **8**, 7873-7882.
8. M. Saghanejhad Tehrani and R. Zare-Dorabei, *RSC Advances*, 2016, **6**, 27416–27425.
9. Z. Wu, X. Wang and J. Qiu, *Separation and Purification Technology*, 2022, **32**, 122078.
10. B. L. Tran, H. Y. Chin, B. K. Chang and A. S. T. Chiang, *Microporous and Mesoporous Materials*, 2019, **277**, 149-153.
11. K. Valizadeh, A. Bateni, N. Sojoodi, R. Rafiei, A. Behroozi and A. Maleki, *International journal of biological macromolecules*, 2023, DOI: 10.1016/j.ijbiomac.2023.123826, 123826.
12. Z. Wu, X. Wang, J. Yao, S. Zhan, H. Li, J. Zhang and Z. Qiu, *Separation and Purification Technology*, 2021, **277**, 119474.